Supplementary Material for

"Electromigration dispersion in a capillary in the presence of electro-osmotic flow"

by

S. Ghosal and Z. Chen

Appendix A. Other Electrokinetic Effects

A.1. *Departures from electroneutrailty in the bulk*

The mathematical formulation presented in Section 2 is based on the premise of local electroneutrality. Since electric fields ($\mathbf{E}$) can only be created by charges, local electroneutrality must necessarily be an approximate rather than an exact constraint. The clearest exposition is achieved in the context of asymptotic theory. In a dimensionless formulation, the problem contains a small parameter $\varepsilon = (\lambda_D/\ell)^2$, where λ_D is the Debye length and ℓ is a characteristic dimension, in terms of which the (dimensionless) electric charge density may be expanded: $\rho = \rho_0 + \varepsilon\rho_1 + \cdots$. Local electroneutrality refers to the fact that $\rho_0 = 0$ in the bulk fluid outside of the Debye layer. However, there is still a small (order ϵ) charge density in the bulk, that under certain conditions could provide a significant body force. This $O(\epsilon)$ charge is associated with conductivity (σ_e) variations as can be seen from a combination of the current ($\mathbf{J}_e$) conservation equation, Ohm's law

$$\boldsymbol{\nabla}\cdot\mathbf{J}_e = \boldsymbol{\nabla}\cdot(\sigma_e\mathbf{E}) = 0$$

and Gauss' law (in a medium with permittivity ϵ_d)

$$\epsilon_d\boldsymbol{\nabla}\cdot\mathbf{E} = -4\pi\rho_e.$$

Thus, we have the charge density

$$\rho_e = -\frac{\epsilon_d}{4\pi}\frac{\boldsymbol{\nabla}\sigma_e\cdot\mathbf{E}}{\sigma_e}.$$

It has been shown (see the papers by Chen *et al.* and Oddy *et al.* in the Reference section) that body forces arising out of such order ε charge density can drive instabilities in certain problems characterized by conductivity variations.

Here we provide an estimate of the possible role of such a small residual charge density in the bulk for our problem. Following the notation of the paper, $\sigma_e = \sigma_\infty[1-\alpha c/c_n^{(\infty)}]^{-1}$, so that

$$\rho_e = -\frac{\epsilon_d}{4\pi}\frac{\boldsymbol{\nabla}\sigma_e\cdot\mathbf{E}}{\sigma_e} = -\frac{\epsilon_d\alpha}{4\pi}\frac{\mathbf{E}\cdot\boldsymbol{\nabla}c}{c_n^{(\infty)}} \sim \frac{\epsilon_d\alpha E_0}{4\pi w_0}.$$

The body force in the channel (per unit span) arising out of such unbalanced charges is

$$f_{bulk} \sim \rho_e E_0 w_0 \sim \frac{\epsilon_d\alpha E_0^2}{4\pi}$$

whereas the net force originating from within the Debye layer is

$$f_{edl} \sim \frac{\epsilon_d\zeta E_0}{4\pi\lambda_D}.$$

Therefore,

$$\frac{f_{bulk}}{f_{edl}} \sim \alpha\frac{E_0 w_0}{\zeta}\frac{\lambda_D}{w_0} \sim 10^{-3}$$

if we use as estimates $\alpha \sim 1$, $E_0 \sim 30$ kV /m, $\zeta \sim 100$ mV, $w_0 \sim 50$ μm and $\lambda_D \sim 10$ nm. Thus, though the force due to the residual bulk charge could be important under certain circumstances, they are generally small compared to the forces arising from the charged Debye layers in the present problem.

A.2. *Diffusiophoretic contribution to electro-osmotic slip*

Diffusiophoresis occurs in systems where there is a variation in the ionic concentration along the slip plane. A mathematical exposition was given Prieve *et al.* cited in References. There are two components that contribute to diffusiophoresis. First, when there is differential diffusion of ions, an electric field arises in order to restore electroneutrality. This electric field then contributes to electro-osmotic slip. Secondly, the pressure forces necessary to maintain equilibrium in the Debye layer varies along the slip plane creating a pressure gradient which contributes to flow in the Debye layer. In our case, the former mechanism is not relevant (the diffusivities being equal) but the latter can still contribute. To estimate the magnitude of the effect, we use Equation (2.22) of the paper by Prieve *et al.* for a binary $Z-Z$ electrolyte (this is sufficent for an estimation, though, strictly speaking we have a three ion system)

$$u_{slip} = -\frac{\epsilon_d}{2\pi\eta}\left(\frac{k_B T}{Ze}\right)^2 \ln(1-\gamma^2)\boldsymbol{\nabla}\ln C_\infty$$

dropping the contribution due to differential diffusion. Here $\gamma = \tanh\left(\frac{Ze\zeta}{4k_B T}\right)$, ϵ_d is the permittivity of the electrolyte, η is its viscosity, k_B is Boltzmann's constant, T is the absolute temperature of the electrolyte, and C_∞ is the concentration field outside of the Debye layer. For convenience, we assume, $\gamma \ll 1$, so that the expression for the slip velocity may be simplified to estimate the diffusiophoretic contribution to the slip:

$$\delta u_{diff} = -\frac{\epsilon_d}{2\pi\eta}\left(\frac{k_B T}{Ze}\right)^2 \ln(1-\gamma^2)\boldsymbol{\nabla}\ln C_\infty \sim \frac{\epsilon_d \zeta^2}{32\pi\eta}\boldsymbol{\nabla}\ln C_\infty \sim \frac{\epsilon_d \alpha \zeta^2}{32\pi\eta w_0}$$

This must be compared to the variation of the Helmholtz-Smoluchowski electro-osmotic slip due to conductivity induced variations of the electric field in the order of αE_0:

$$\delta u_{eof} \sim \frac{\epsilon_d \zeta \alpha E_0}{4\pi\eta}.$$

Thus, the ratio

$$\frac{\delta u_{diff}}{\delta u_{eof}} \sim \frac{\zeta}{8E_0 w_0} \sim 0.008$$

if we use the estimates $E_0 \sim 30$ kV/m, $w_0 \sim 50$ μm, $\zeta \sim 100$ mV. Thus, the diffusiophoretic contribution is typically small and may be ignored, except when the ratio $\zeta/(E_0 w_0)$ happens to be of order unity or larger.

Appendix B. Details of Numerical Computations

Equation (3.23) is the main result of the paper. To solve it, the dimensionless form was used:

$$\frac{\partial\bar{\phi}}{\partial\tilde{t}} + \frac{\partial}{\partial\tilde{x}}\left[\left(u_* + \frac{1}{1-\alpha\bar{\phi}}\right)\bar{\phi}\right] = \frac{\partial}{\partial\tilde{x}}\left(D_{\text{eff}}\frac{\partial\bar{\phi}}{\partial\tilde{x}}\right) \tag{B 1}$$

where $\tilde{t} = v_0 t/w_0$, $\tilde{x} = x/w_0$, $u_* = u_{eo}/v_0$ and $D_{\text{eff}} = Pe^{-1} + ku_*^2 Pe\left(\frac{\alpha\bar{\phi}}{1-\alpha\bar{\phi}}\right)^2$. The equation can be further simplified by transforming to a reference frame moving with the

constant velocity $u_* + 1$:

$$\frac{\partial \bar{\phi}}{\partial \tilde{t}} + \frac{\partial}{\partial \tilde{x}} \left[\left(\frac{1}{1 - \alpha \bar{\phi}} - 1 \right) \bar{\phi} \right] = \frac{\partial}{\partial \tilde{x}} \left(D_{\text{eff}} \frac{\partial \bar{\phi}}{\partial \tilde{x}} \right). \tag{B 2}$$

Equation (B 2) was the one actually solved numerically.

Since the peak could display sharp fronts, adaptive grid refinement was used in order to enable fine grids in the region of sharp gradients while keeping the total number of grid points modest. The Matlab library "Matmol" was applied for this purpose. This library provides a user-friendly solution for implementing adaptive grids in PDE models. The subroutine examines the concentration distribution at pre-determined intervals (for example every 50 steps) and evaluates a "monitor function" based on some measure of sharpness of the profile such as the absolute value of the derivative or the curvature. When preset limits are exceeded, a new grid is generated and the concentration interpolated on to the new grid points.

The finite volume method is used for discretizing space. Thus, Equation (B 2) is first written in conservative form

$$\frac{\partial \bar{\phi}}{\partial \tilde{t}} = \frac{\partial}{\partial \tilde{x}} \left[- \left(\frac{1}{1 - \alpha \bar{\phi}} - 1 \right) \bar{\phi} + D_{\text{eff}} \frac{\partial \bar{\phi}}{\partial \tilde{x}} \right]. \tag{B 3}$$

Integrating over a grid interval then reduces it to a system of ode's. This is the so called method of lines (MOL) technique. For the integration on time the MATLAB solver "ode15s" was used (See Shampine, & Reichelt in the Reference section). The solver is designed for stiff problems and enables variable marching steps determined by user specified absolute and relative tolerances. We set these parameters at *Reltol = 1.0e-6*, *Abstol = 1.0e-9*.

To validate the code, the case of pure diffusion, that is, $\alpha = 0$ in Equation (B 3), was tested first. The compute domain was set as $x = [0\ 120]$. The system was initialized with a Gaussian peak: centroid at $x = 40$, variance 1 and peak height 0.1. The code provides a parameter, "tolx" determining the grid quality. The smaller tolx is, the finer the grid will be. To check grid independence, the same test case was run twice, once with *tolx = 1e-3*, and again with *tolx = 2e-3* (Figure 1). The numerical results agree well with each other and with the well known analytical solution (the Fourier law of diffusion). Next, a test case using the full Equation (B 2) was run with $\alpha = 0.5$, $Pe = 200$ and $u_* = 10$ (Figure 1). Once again, no grid dependence is seen between *tolx = 1e-3* and the coarser grid *tolx = 2e-3*. The adaptive grid setting was therefore set to *tolx = 1e-3* for all the other cases.

Appendix C. Alternate Representations of Simulation Results

In this section we provide some additional graphs obtained from the numerical solution of Equation (3.23) to complement the ones already presented in the paper.

Figure 2 presents the same data as Figure 2 in the paper. However, instead of the rate of increase of variance, the variance itself is shown as a function of time. Since the curves are a bit difficult to tell apart, in the bottom panel we show the difference between the variance with a given value of u_* with a reference case where $u_* = 0$. Figure 3 shows the increase of variance with time at different sample loadings, for a fixed value of the flow, $u_* = 2$. Clearly the variance is higher the greater the sample loading as one would expect. In Figure 4 we present the same data presented in Figure 3 of the paper but plotted in a different way. We show how N changes with the capillary length L when the electric field

is kept fixed. It is seen that $N \propto L$† which is the classical result. However, the slope of these N vs. L curves depend on the sample loading (P) and the flow rate (u_*). Generally, higher P correspond to smaller slopes. Figure 5 is similar, but it shows how the variance itself increases with time. Figure 6 provides an alternate way of looking at Figure 5 in the paper. Here instead of plotting $\bar{\phi}$ as a function of time at a fixed detector location, we show $\bar{\phi}$ as a function of axial distance at fixed times.

† if the voltage was kept fixed instead, this would correspond to N being independent of L.

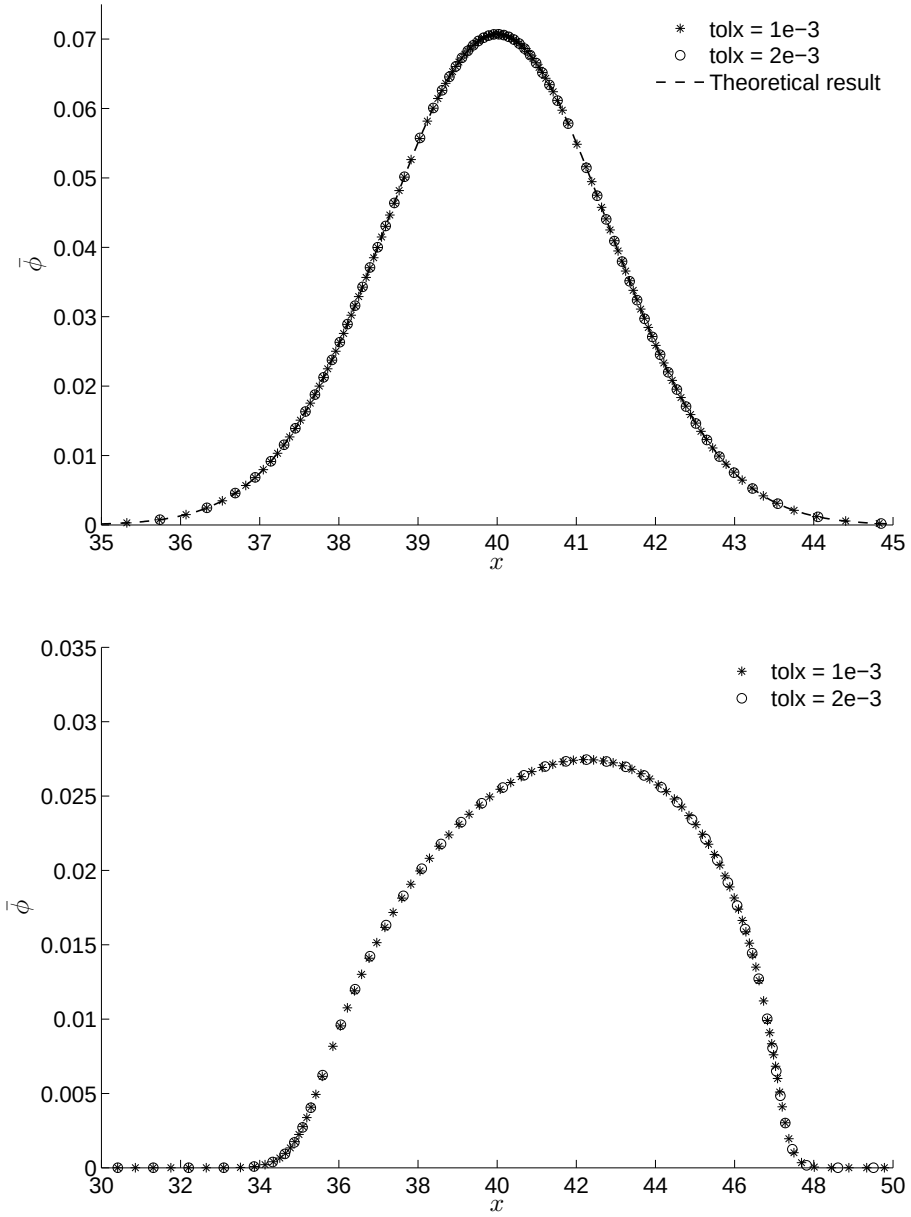

FIGURE 1. Tests of numerical accuracy showing computed concentration profiles at a fixed dimensionless time $\tilde{t} = 100$. Parameters are (Upper panel): $Pe = 200$, $\alpha = 0$ corresponding to pure diffusion with diffusivity Pe^{-1}. (Lower panel): $Pe = 200$, $\alpha = 0.5$ and $u_* = 10$. There is no discernible difference between the solutions obtained with the coarse and fine grid. Furthermore, in the pure diffusion case, the numerical computation agrees well with the analytical solution for the diffusion problem (Fourier's solution).

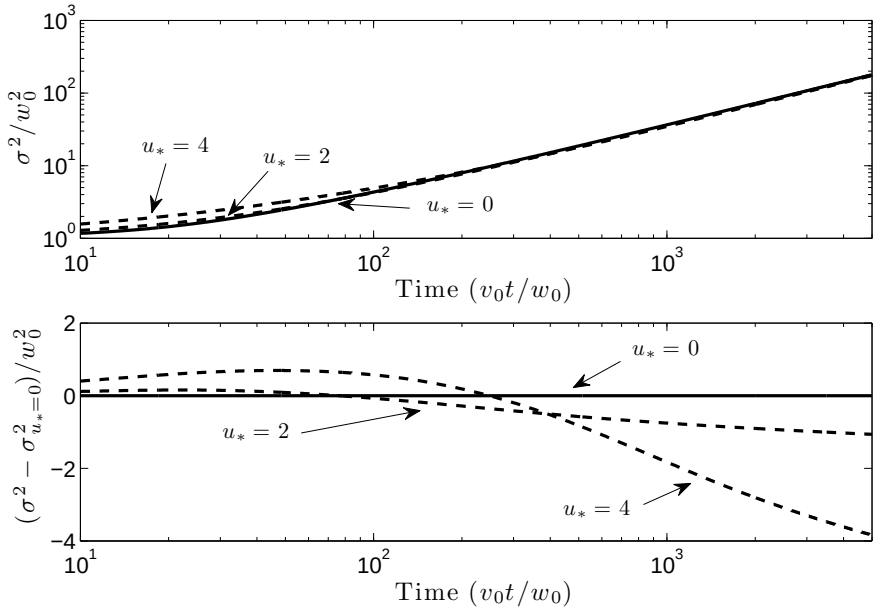

FIGURE 2. Time evolution of the variance (upper panel) for three different values of the dimensionless electro-osmotic flow strength $u_* = u_{eo}/v_0 = 0, 2$ and 4. In the lower panel the difference in the variance between the indicated value of u_* and the case with $u_* = 0$ is shown. Electro-osmotic flow results in an initial increase in the variance but a drop in the variance at later times.

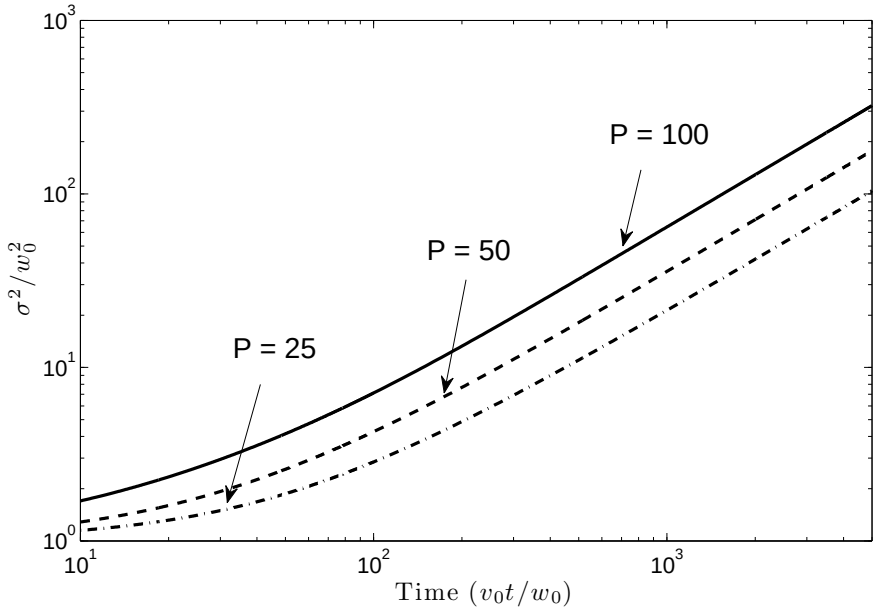

FIGURE 3. The dependence of the variance on the sample loading as measured by the Peclet number (P). The dimensionless electro-osmotic flow strength $u_* = u_{eo}/v_0 = 2$ is kept fixed. Electromigration dispersion causes the variance at a given time to be larger for higher values of P.

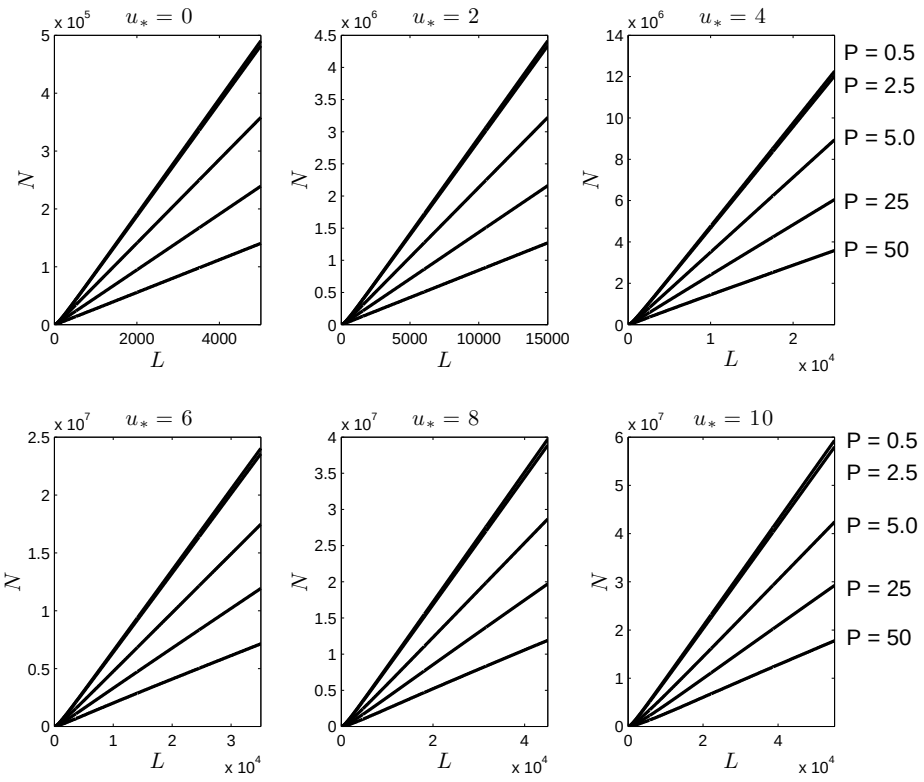

FIGURE 4. The number of theoretical plates $N = L^2/\sigma^2$ as a function of the injection to detection distance, L for different values of the dimensionless electro-osmotic velocity $u_* = u_{eo}/v_0$ and sample loading measured by the Peclet number, P. The applied electric field is kept fixed when L is varied.

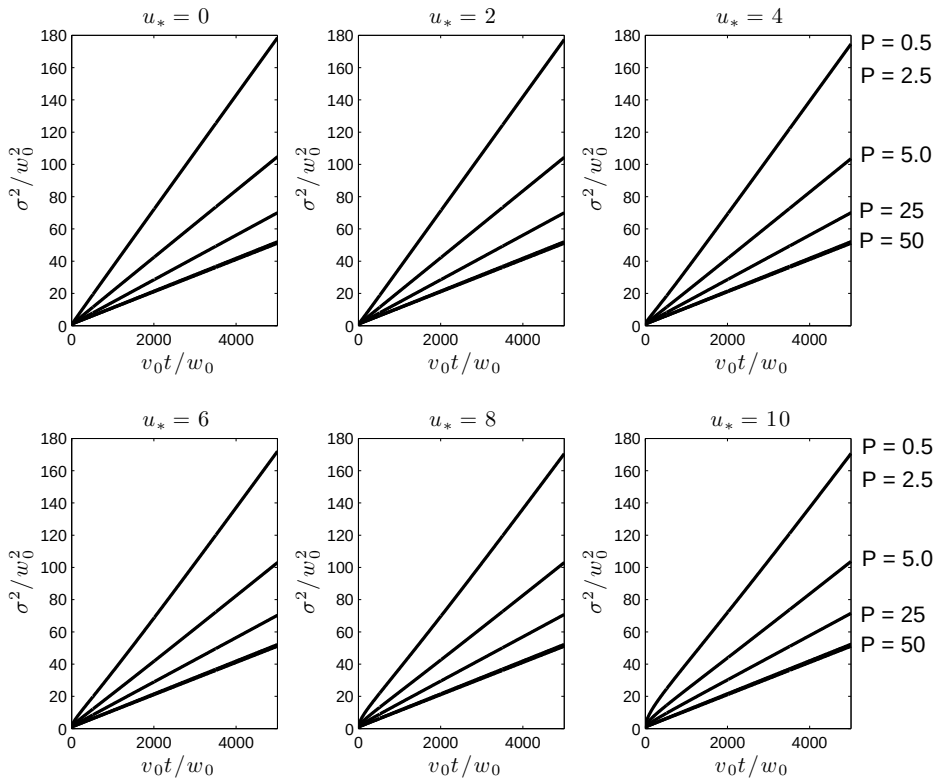

FIGURE 5. The normalized variance, σ_0^2/w_0^2, as a function of the dimensionless time $v_0 t/w_0$ for different values of the dimensionless electro-osmotic velocity, $u_* = u_{eo}/v_0$ and sample loading measured by the Peclet number, P.

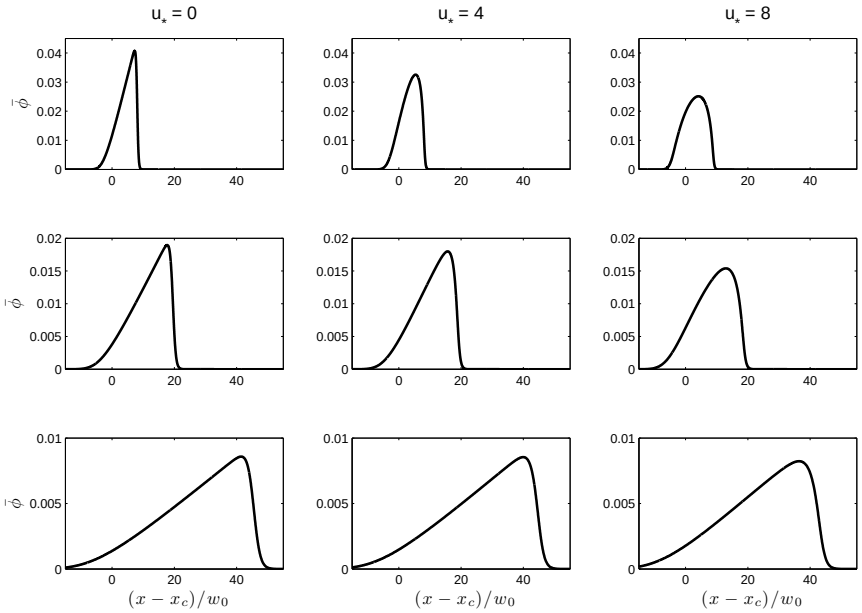

FIGURE 6. Concentration profiles at fixed dimensionless times: $v_0 t/w_0 = 200$ (upper panel), 1000 (middle panel) and 5000 (lower panel), for several values of u_*. The Peclet number, $P = 50$. Here x_c is the location of the centroid in the reference case with $\alpha = 0$, that is, in the absence of electromigration dispersion.